Acta Crystallographica Section B
Structural Science
ISSN 0108-7681

Effect of pressure on the crystal structure of salicylaldoxime-I, and the structure of salicylaldoxime-II at 5.93 GPa

Peter A. Wood,[a] Ross S. Forgan,[a] David Henderson,[a] Simon Parsons,[a]* Elna Pidcock,[b] Peter A. Tasker[a] and John E. Warren[c]

[a]School of Chemistry and Centre for Science at Extreme Conditions, The University of Edinburgh, King's Buildings, West Mains Road, Edinburgh EH9 3JJ, Scotland, [b]Cambridge Crystallographic Data Centre, 12 Union Road, Cambridge CB2 1EZ, England, and [c]CCLRC, Daresbury Laboratory, Warrington, Cheshire WA4 4AD, England

Correspondence e-mail: s.parsons@ed.ac.uk

Received 3 June 2006
Accepted 11 August 2006

The effect of pressure on the crystal structure of salicylaldoxime has been investigated. The ambient-pressure phase (salicylaldoxime-I) consists of pairs of molecules interacting through oximic OH···O hydrogen bonds; taken with phenolic OH···N intramolecular hydrogen bonds, these dimers form a pseudo-macrocycle bounded by an $R_4^4(10)$ motif. The dimers interact principally *via* $\pi\cdots\pi$ stacking contacts. Salicylaldoxime derivatives are used industrially as selective solvent extractants for copper; the selectivity reflects the compatibility of the metal ion with the pseudo-macrocycle cavity size. On increasing the pressure to 5.28 GPa the size of the cavity was found to decrease by an amount comparable to the difference in hole sizes in the structures of the Cu^{2+} salicylaldoximato complex and its Ni^{2+} equivalent. On increasing the pressure to 5.93 GPa a new polymorph, salicylaldoxime-II, was obtained in a single-crystal to single-crystal phase transition. PIXEL calculations show that the phase transition is driven in part by relief of intermolecular repulsions in the dimer-forming OH···O-bonded ring motif, and the ten-centre hydrogen-bonding ring motif of the phase I structure is replaced in phase II by a six-centre ring formed by oximic OH···N hydrogen bonds. The transition also relieves repulsions in the $\pi\cdots\pi$ stacking contacts. The intramolecular OH···N hydrogen bond of phase I is replaced in phase II by a intermolecular phenolic OH···O hydrogen bond, but the total interaction energy of the pairs of molecules connected by this new contact is very slightly repulsive because the electrostatic hydrogen-bond energy is cancelled by the repulsion term. The intra- to intermolecular hydrogen-bond conversion simply promotes efficient packing rather than contributing to the overall lattice energy.

1. Introduction

The use of high pressure as a probe for studying molecular crystal structures under non-ambient conditions is still relatively lightly explored compared with low-temperature studies. Recent studies of small organic molecules (Dawson *et al.*, 2005; Moggach, Allan, Morrison *et al.*, 2005; Moggach *et al.*, 2006) have found that the primary effect of compression in these cases is to reduce the sizes of voids present in the ambient-pressure structure. Analysis of the distributions and sizes of voids in crystal structures at ambient and high pressures is therefore an important area of research in terms of understanding the effects of compression. The subject of the effect of pressure on molecular systems has been addressed in a number of recent reviews, for example Boldyreva (2003, 2004*a*,*b*), Katrusiak (2004) and Hemley & Dera (2000).

The presence of voids in a structure may also be of importance in the determination of chemical reactivity. Most of the voids in the crystal structure of a small organic compound will be between molecules, but some compounds also have intramolecular voids (usually referred to as *cavities*). One example of this phenomenon is 18-crown-6, which has a large cavity inside the ring of the molecule and is known to form complexes with metal ions such as Na^+, K^+ and Rb^+. The type of complexation in these complexes is dependent on the size of the metal ion in relation to the crown ether cavity size. In the case of 18-crown-6 the macrocyclic cavity is best suited to the K^+ cation, but it can also form complexes with smaller or larger cations by distorting the conformation of the molecule or by complexing the cation with two crown ether molecules in a 'sandwich' arrangement (Gokel, 1991).

Salicylaldoxime [Scheme (I)] forms a hydrogen-bonded dimer creating a pseudo-macrocyclic cavity in the middle of the hydrogen-bonded *R*-type ring motif [Scheme (II*a*)] (Bernstein *et al.*, 1995). Deprotonation of the phenol group enables salicylaldoxime to bind to a transition metal as a mono-anionic, bidentate ligand. A bis(salicylaldoxime) complex is stabilized by hydrogen bonding between the two bidentate ligands.

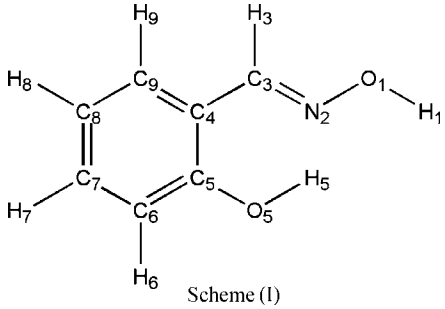

Scheme (I)

Salicylaldoxime is known to show a remarkable selectivity for complex formation of copper(II) above other metal ions as a result of the compatibility of the size of the cavity at the centre of the *R* motif and the ionic radius of Cu^{2+} (Smith *et al.*, 2002). Salicylaldoximes bearing branched alkyl chains are used as solvent extractants to effect the 'separation' and 'concentration' operations in the hydrometallurgical recovery of copper, accounting for around 30% of annual production (Kordosky, 2002). The high affinity and selectivity of salicylaldoximes for Cu^{2+} is therefore of great commercial importance (Szymanowski, 1993).

The development of ligands suitable for the selective complexation of metal ions based on synthesizing derivatives to control cavity sizes in polydentate ligands is both time-consuming and costly (Tasker *et al.*, 2004). As salicylaldoximes are predisposed to assemble to provide $N_2O_2^{2-}$ cavities for metal ions, an attractive alternative strategy would be to control the size of the cavity using pressure, and in this paper we discuss the effect of pressure to 6 GPa on the crystal structure of salicylaldoxime.

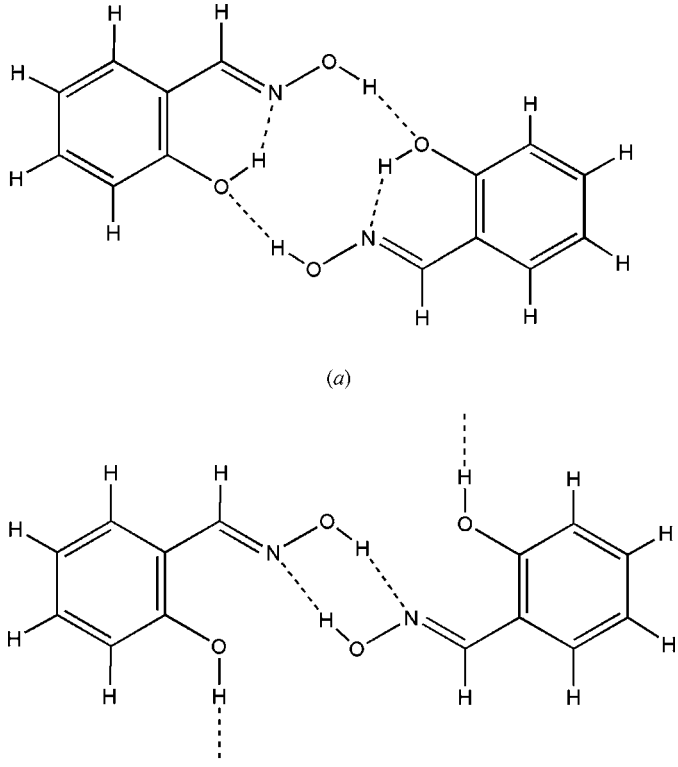

(*a*)

(*b*)

Scheme (II)

2. Experimental

2.1. Crystal growth

Salicylaldoxime (98%) was purchased from Acros (CAS number 94-67-7); it was then recrystallized by the slow evaporation of a concentrated hexane/chloroform solution. One small, colourless, block-shaped crystal was then taken directly from the recrystallized sample. The unit-cell dimensions of the crystal were determined at 150 K and ambient pressure to be monoclinic, a = 10.359 (3), b = 5.007 (1), c = 13.292 (3) Å, β = 112.14 (2)°. The structure of salicylaldoxime has previously been reported by Pfluger & Harlow (1973), and we refer to this phase as *salicyladoxime-I*. The same crystal was then loaded into a diamond–anvil cell.

2.2. High-pressure crystallography

High-pressure experiments were carried out using a Merrill–Bassett diamond–anvil cell (half-opening angle 40°), equipped with brilliant-cut diamonds with 600 µm culets and a tungsten gasket (Merrill & Bassett, 1974). A 1:1 mixture of *n*-pentane and isopentane was used as a hydrostatic medium; this mixture is volatile at room temperature, and the cell was cooled in dry ice prior to loading. A small ruby chip was also loaded into the cell so that the pressure could be monitored using the ruby fluorescence method (Piermarini *et al.*, 1975). Diffraction data were collected on a Bruker–Nonius APEX-II

diffractometer with silicon-monochromated synchrotron radiation (λ = 0.6889 Å) on Station 9.8 at the SRS, Daresbury Laboratory.

Data collection and processing procedures for the high-pressure experiments followed Dawson *et al.* (2004) and Moggach, Allan, Parsons *et al.* (2005). Integrations were carried out using the program *SAINT* (Bruker–Nonius, 2003), and absorption corrections with the programs *SHADE* (Parsons, 2004) and *SADABS* (Sheldrick, 2004). Data collections were taken in approximately 1.0 GPa steps from 0.75 GPa up to a final pressure of 5.93 GPa. Determination of the cell constants at 5.93 GPa showed that a single-crystal to single-crystal phase transition had occurred to a new polymorph, which we have designated *salicylaldoxime-II*. The phase transition degraded the crystal quality somewhat, and no attempt was made to study the effects of subsequent decompression.

In order to facilitate a comparison with the ambient-temperature/high-pressure results, diffraction data were also collected on salicylaldoxime-I at ambient pressure. Data were collected on a Bruker APEX diffractometer with graphite-monochromated Mo $K\alpha$ radiation (λ = 0.71073 Å). The crystals were sensitive to radiation damage from the X-ray beam, so this data set was collected at 273 K. The data were integrated using *SAINT* and corrected for absorption with *SADABS*. The structure was solved using the program *SIR*92 (Altomare *et al.*, 1994) and structure refinement yielded a conventional *R* factor of 0.0564, giving structural parameters that are somewhat more precise than those determined by Pfluger & Harlow (1973).

Refinements of the compressed form of salicylaldoxime-I were carried out starting from the coordinates determined at ambient pressure. The structure of the new phase (salicylaldoxime-II) was solved by direct methods using the program *SIR*92. Refinements were carried out against $|F|^2$ using all data (*CRYSTALS*; Betteridge *et al.*, 2003). Owing to the low completeness of the data sets, global rigid-bond and body restraints were applied to the anisotropic displacement parameters. The quality of the diffraction pattern deteriorated markedly after the transformation to salicylaldoxime-II, and no attempt was made to study this sample at still higher pressures. Displacement parameters in phase II were only modelled at the isotropic level; shift-limiting restraints were also applied to all parameters.

H atoms attached to C atoms were placed geometrically and constrained to ride on their host C atoms. The hydroxyl H atoms (H1 and H5) in all cases were found using difference-Fourier maps. The positional parameters of atoms H1 and H5 were then refined subject to the restraint O—H = 0.820 (1) Å. Listings of crystal and refinement data are given in Table 1.[1]

Crystal structures were visualized using the programs *CAMERON* (Watkin *et al.*, 1993), *MERCURY* (Bruno *et al.*, 2002) and *DIAMOND* (Brandenburg & Putz, 2005). Analyses were carried out using *PLATON* (Spek, 2004), as incorporated in the *WinGX* suite (Farrugia, 1999). Searches of the Cambridge Structural Database (CSD; Allen, 2002; Allen & Motherwell, 2002) utilized the program *CONQUEST* and version 5.27 of the database with updates up to January 2006.

Topological calculations of void distributions (Blatov & Shevchenko, 2003) were carried out with *TOPOS-Pro* (Blatov *et al.*, 1995, 2000). Considerable simplification of the void distributions can be gained by clustering; voids were therefore clustered using what the program refers to as the 'clustering' method with the 'size' parameter specified as 0.5 (Blatov, 2005). Strain tensor calculations were carried out using a locally written program (*STRAIN*; Parsons, 2003), based on the discussion in Hazen & Finger (1982) and employing the *JACOBI* subroutine of Press *et al.* (1992). Equation-of-state calculations were carried out with *EOSFIT* (Angel, 2002).

The numbering scheme used [see Scheme (I)] is the same throughout the ambient-pressure and high-pressure data sets, including the phase II structure. The setting that was used for the salicylaldoxime-II structure was chosen to facilitate the comparison with salicylaldoxime-I.

2.3. PIXEL calculations

The final crystal structures obtained were used to calculate the molecular electron density at each pressure by standard quantum chemical methods using the program *GAUSSIAN*98 (Frisch *et al.*, 1998) at the MP2/6-31G** level of theory. H-atom distances were set to standard neutron values (C—H = 1.083 and O—H = 0.983 Å). The electron-density model of the molecule was then analysed using the program package *OPiX* (Gavezzotti, 2005), which allowed the calculation of dimer and lattice energies. Lattice energy calculations employed a cluster of molecules of radius 18 Å. Calculations were also carried out for pairs of molecules identified in the lattice calculation as being energetically the most significant (*i.e.* with a magnitude > 2.5 kJ mol^{-1}). The output from these calculations yields a total energy and a breakdown into its electrostatic, polarization, dispersion and repulsion components (Dunitz & Gavezzotti, 2005).

3. Results

3.1. The structure of salicylaldoxime-I at ambient pressure

Prior to this work two crystalline forms of salicylaldoxime had been characterized. The structure of salicylaldoxime-I was determined by Pfluger & Harlow (1973); salicylaldoxime-III was initially studied by Merritt & Schroeder (1956), but its structure was determined only recently (Wood *et al.*, 2006). The crystal structure of salicylaldoxime-I has one molecule in the asymmetric unit in the space group $P2_1/n$. The molecule as a whole is planar; a least-squares mean plane calculated using the C, N and O atoms shows that the average deviation of these atoms from the plane is 0.009 Å.

The molecules form intramolecular O5—H5···N2 hydrogen bonds [O5···N2 = 2.621 (2) Å] and intermolecular O1—H1···O5 hydrogen bonds [O1···O5 = 2.793 (2) Å]. The

[1] Supplementary data for this paper are available from the IUCr electronic archives (Reference: SO5004). Services for accessing these data are described at the back of the journal.

Table 1
Crystallographic data for salicylaldoxime at increasing pressures.

	Ambient	0.75 GPa	2.37 GPa	3.46 GPa	4.55 GPa	5.28 GPa	5.93 GPa
Crystal data							
Chemical formula	$C_7H_7NO_2$	$C_7H_7NO_2$	$C_7H_7NO_2$	$C_7H_7NO_2$	$C_7H_7NO_2$	$C_7H_7NO_2$	$C_7H_7NO_2$
M_r	137.14	137.14	137.14	137.14	137.14	137.14	137.14
Cell setting, space group	Monoclinic, $P2_1/n$	Monoclinic, $P2_1/n$	Monoclinic, $P2_1/n$	Monoclinic, $P2_1/n$	Monoclinic, $P2_1/n$	Monoclinic, $P2_1/n$	Monoclinic, $P2_1/n$
Temperature (K)	273	293	293	293	293	293	293
a, b, c (Å)	10.346 (4), 5.0294 (17), 13.478 (5)	10.1833 (16), 4.9766 (3), 13.0109 (15)	9.851 (3), 4.9325 (7), 12.286 (3)	9.7148 (16), 4.9322 (3), 12.0145 (16)	9.5728 (15), 4.9342 (3), 11.7537 (15)	9.513 (2), 4.9319 (4), 11.630 (2)	7.677 (3), 5.7731 (8), 12.159 (3)
β (°)	112.21 (2)	111.938 (10)	111.09 (2)	110.607 (11)	110.064 (10)	109.859 (14)	110.62 (2)
V (Å^3)	649.3 (4)	611.62 (13)	557.0 (3)	538.84 (12)	521.48 (11)	513.19 (15)	504.4 (3)
Z	4	4	4	4	4	4	4
D_x (Mg m^{-3})	1.403	1.489	1.635	1.690	1.747	1.775	1.806
Radiation type	Mo $K\alpha$	Synchrotron	Synchrotron	Synchrotron	Synchrotron	Synchrotron	Synchrotron
μ (mm^{-1})	0.10	0.11	0.12	0.13	0.13	0.13	0.13
Crystal form, colour	Block, colourless	Block, colourless	Block, colourless	Block, colourless	Block, colourless	Block, colourless	Block, colourless
Crystal size (mm)	0.26 × 0.10 × 0.10	0.18 × 0.15 × 0.10	0.18 × 0.15 × 0.10	0.18 × 0.15 × 0.10	0.18 × 0.15 × 0.10	0.18 × 0.15 × 0.10	0.18 × 0.15 × 0.10
Data collection							
Diffractometer	Bruker SMART APEX CCD	Bruker–Nonius APEX II CCD	Bruker–Nonius APEX II CCD	Bruker–Nonius APEX II CCD	Bruker–Nonius APEX II CCD	Bruker–Nonius APEX II CCD	Bruker–Nonius APEX II CCD
Data collection method	ω	ω	ω	ω	ω	ω	ω
Absorption correction	Multi-scan (based on symmetry-related measurements)	Multi-scan (based on symmetry-related measurements)	Multi-scan (based on symmetry-related measurements)	Multi-scan (based on symmetry-related measurements)	Multi-scan (based on symmetry-related measurements)	Multi-scan (based on symmetry-related measurements)	Multi-scan (based on symmetry-related measurements)
T_{min}	0.79	0.34	0.51	0.62	0.38	0.42	0.46
T_{max}	0.99	0.99	0.99	0.99	0.99	0.99	0.99
No. of measured, independent and observed reflections	6424, 1982, 1019	2288, 547, 335	2109, 472, 309	2031, 412, 317	1793, 417, 285	1925, 410, 305	1157, 296, 191
Criterion for observed reflections	$I > 2\sigma(I)$	$I > 2\sigma(I)$	$I > 2\sigma(I)$	$I > 2\sigma(I)$	$I > 2\sigma(I)$	$I > 2\sigma(I)$	$I > 2\sigma(I)$
R_{int}	0.047	0.079	0.075	0.061	0.069	0.076	0.126
θ_{max} (°)	30.7	26.8	26.4	26.4	26.4	26.4	23.3
Refinement							
Refinement on	F^2	F^2	F^2	F^2	F^2	F^2	F^2
$R[F^2 > 2\sigma(F^2)]$, $wR(F^2)$, S	0.056, 0.175, 0.92	0.049, 0.136, 0.79	0.040, 0.101, 0.89	0.042, 0.107, 0.88	0.044, 0.112, 0.91	0.041, 0.094, 0.94	0.125, 0.275, 0.82
No. of reflections	1982	514	437	412	394	386	268
No. of parameters	97	97	97	97	97	97	47
H-atom treatment	Mixture of independent and constrained refinement	Mixture of independent and constrained refinement	Mixture of independent and constrained refinement	Mixture of independent and constrained refinement	Mixture of independent and constrained refinement	Mixture of independent and constrained refinement	Mixture of independent and constrained refinement
Weighting scheme	$w = 1/[\sigma^2(F^2) + (0.09P)^2 + 0.04P]$ where $P = [\max(F_o^2,0) + 2F_c^2)/3$	Calculated method, Chebychev polynomial, with a robust resistant modifier (Watkin, 1994; Prince, 1982)	Calculated method, Chebychev polynomial, with a robust resistant modifier (Watkin, 1994; Prince, 1982)	Calculated method, Chebychev polynomial, with a robust resistant modifier (Watkin, 1994; Prince, 1982)	Calculated method, Chebychev polynomial, with a robust resistant modifier (Watkin, 1994; Prince, 1982)	Calculated method, Chebychev polynomial, with a robust resistant modifier (Watkin, 1994; Prince, 1982)	Calculated method, Chebychev polynomial, with a robust resistant modifier (Watkin, 1994; Prince, 1982)
$(\Delta/\sigma)_{max}$	<0.0001	<0.0001	<0.0001	<0.0001	<0.0001	<0.0001	<0.0001
$\Delta\rho_{max}$, $\Delta\rho_{min}$ (e Å^{-3})	0.25, −0.23	0.11, −0.11	0.09, −0.16	0.13, −0.14	0.14, −0.12	0.13, −0.11	0.37, −0.40
Extinction method	None	None	None	None	None	None	None

Computer programs used: *APEX*-II (Bruker–Nonius, 2000), *SAINT* (Bruker–Nonius, 2003), *SIR*92 (Altomare *et al.*, 1994), *CRYSTALS* (Betteridge *et al.*, 2003), *CAMERON* (Watkin *et al.*, 1993).

latter form a dimer across an inversion centre (Fig. 1*a*), yielding a ring motif for which the graph-set descriptor is $R_4^4(10)$ (Bernstein *et al.*, 1995). The two molecules in the dimer are almost coplanar, with a distance of only 0.28 Å between the two least-squares planes. The H atom (H1) that forms a hydrogen bond across the dimer lies 0.09 (2) Å from the mean plane of the molecule.

The molecule has three hydrogen-bond acceptors (O1, N2 and O5) and only two conventional donors (O1/H1 and O5/H5), and there is therefore an unfulfilled hydrogen-bond acceptor (based on O1). Atom O1 forms a very weak inter-dimer C6—H6···O1 interaction with a neighbouring molecule [C6···O1 = 3.404(2) Å, PIXEL energy = −2.7 kJ mol^{-1} (Fig. 2*a*)]. Successive C6—H6···O1 interactions related by the *n*-glide build primary-level *C*(7) chains, producing 'slabs' which lie in the (10$\bar{1}$) plane (Fig. 3*a*). There are no hydrogen-bond interactions between the slabs.

Within the slabs, dimers interact with other dimers through $\pi\cdots\pi$ stacking (Fig. 4). The inter-plane separations are 3.07 and 3.40 Å between the reference molecule and the molecules labelled 2 and 3, respectively. We show below that these stacking interactions are in fact more energetically significant than the CH···O contacts. The centroids of the phenyl rings are off-set from each other by 3.71 and 5.25 Å for these two interactions along the horizontal direction in Fig. 4, and the stacking interaction appears to be between $R_4^4(10)$ and phenyl rings.

3.2. The response of salicylaldoxime-I to pressure up to 5.28 GPa

The response of the salicylaldoxime-I structure to hydrostatic pressure is anisotropic (Fig. 5); the greatest reduction occurs in the *c*-axis length (13.7% at 5.28 GPa relative to ambient pressure), while the *a* and *b* axes reduce by 8.1 and 1.9%, respectively. The direction of greatest linear strain lies approximately along the reciprocal axis direction (10$\bar{2}$); the principal axis with the second largest eigenvalue is approximately along (601). These directions are shown in Fig. 6. One eigenvector of the strain tensor must correspond to the *b* direction by symmetry, and this is the direction of least compression in the structure.

The bulk modulus (K_0), refined for a Birch–Murnaghan equation-of-state (Birch, 1947; Angel, 2000) to second order, is 13.3 (4) GPa. The data set used to calculate this quantity is admittedly rather limited, and the values of V_0 and K' were fixed at 649.3 Å^3 and 4, respectively. Molecular solids typically have K_0 < 30 GPa (Angel, 2004); Slebodnick *et al.* (2004) quote the following K_0 values which are useful for comparison: $Ru_3(CO)_{12}$ (6.6 GPa), NaCl (25 GPa), quartz (37 GPa), ceramics (50–300 GPa) and diamond (440 GPa).

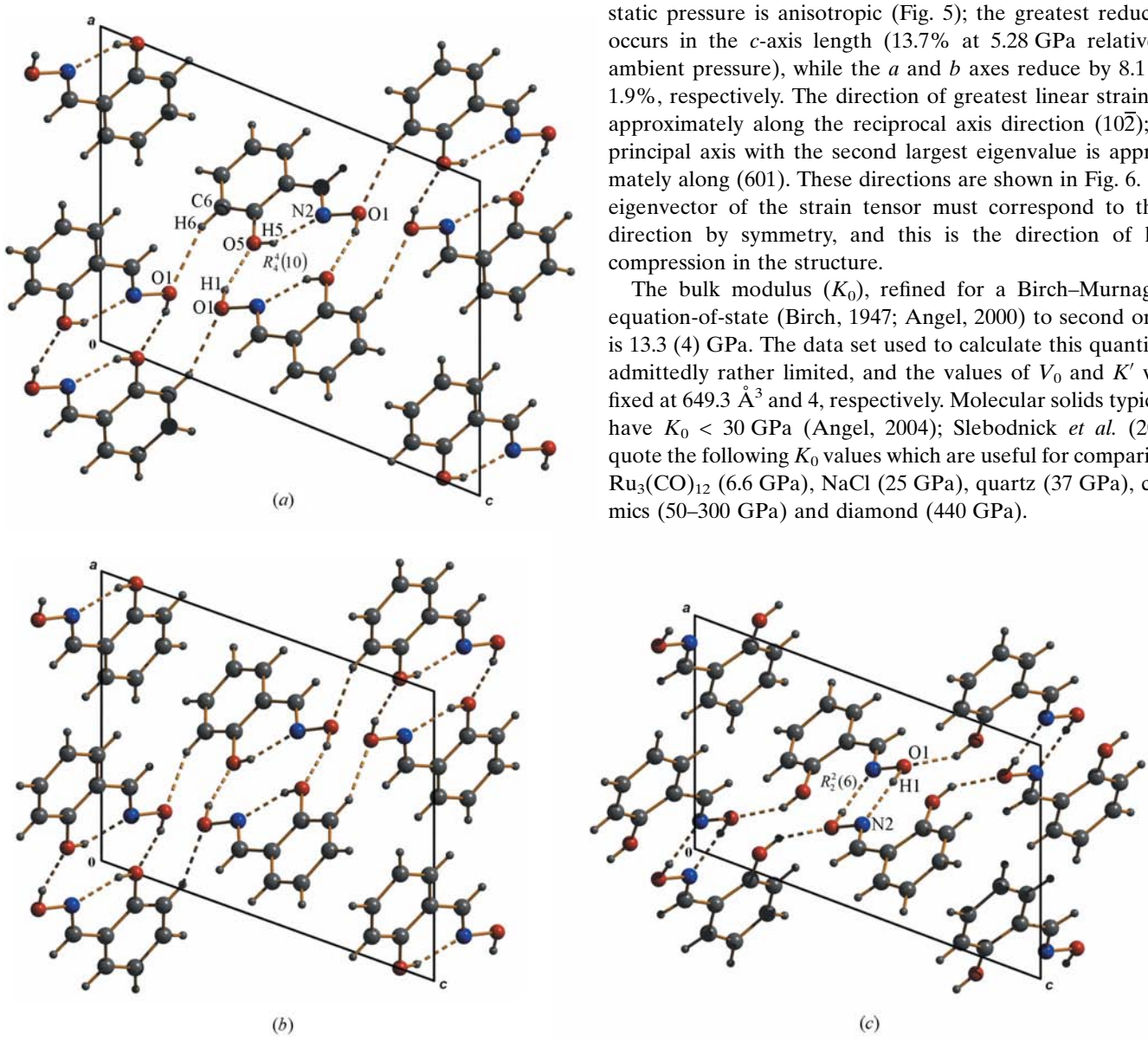

Figure 1
The effect of pressure on the crystal structure of salicylaldoxime as viewed along *b*: (*a*) salicylaldoxime-I at ambient pressure; (*b*) salicylaldoxime-I at 5.28 GPa; (*c*) salicylaldoxime-II at 5.93 GPa. The colour scheme is red: oxygen, blue: nitrogen, light-grey: carbon and dark-grey: hydrogen.

The molecule remains planar at 5.28 GPa, and the distance between the least-squares planes of the molecules in the dimer remains essentially constant (0.27 Å at 5.28 GPa).

The variation of non-covalent interaction parameters in salicylaldoxime-I between ambient pressure and 5.28 GPa is presented in Table 2. The least compressible interaction is the intramolecular OH···N hydrogen bond from O5/H5 to N2 (O5···N2 changes by 2.2%). The second conventional hydrogen bond (O1/H1···O5) is significantly more compressible because of the greater spatial flexibility of the molecules; O1···O5 decreases by 6.5% to a distance of 2.612 (6) Å. The OH···O angle remains approximately constant, and so the shape of the hydrogen-bonding ring is essentially unchanged (*cf.* Figs. 1*a* and 1*b*). The most compressible hydrogen-bonding interaction is C6—H6···O1 which decreases by 9.6% to 3.077 (9) Å. The CHO angle decreases steadily with the application of pressure from 154 to 146° at 5.28 GPa as the molecules shift with respect to each other in order to pack more effectively (see Figs. 1 and 2).

The $\pi\cdots\pi$ stacking interaction distances, defined as the perpendicular distance between the least-squares mean plane of one phenyl ring and the centroid of another, are also

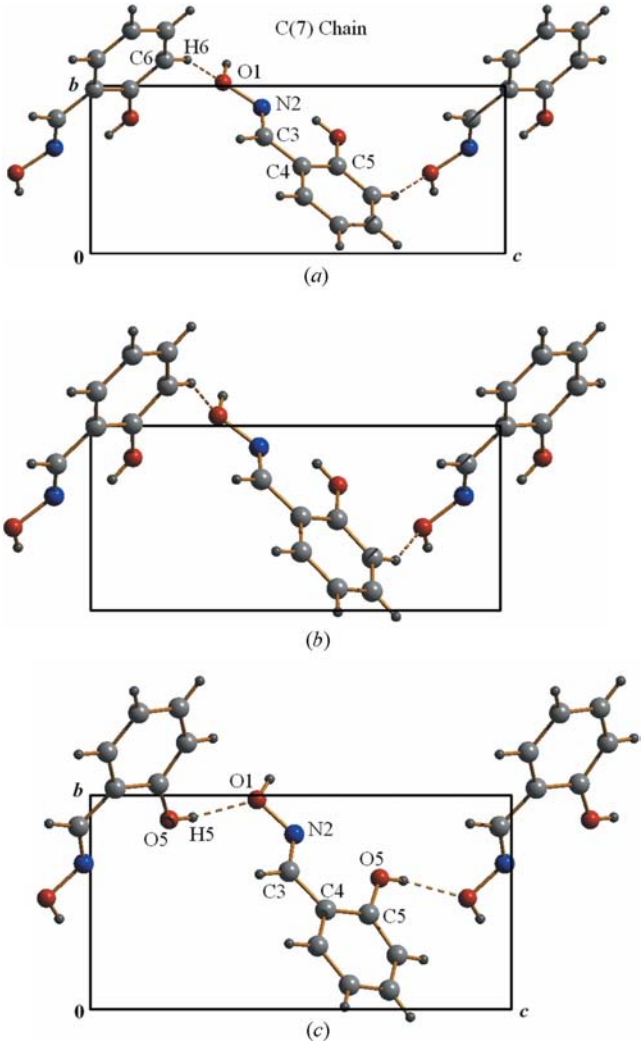

Figure 2
The effect of pressure on the crystal structure of salicylaldoxime as viewed along *a*: (*a*) salicylaldoxime-I at ambient pressure; (*b*) salicylaldoxime-I at 5.28 GPa; (*c*) salicylaldoxime-II at 5.93 GPa. The colour scheme is the same as in Fig. 1.

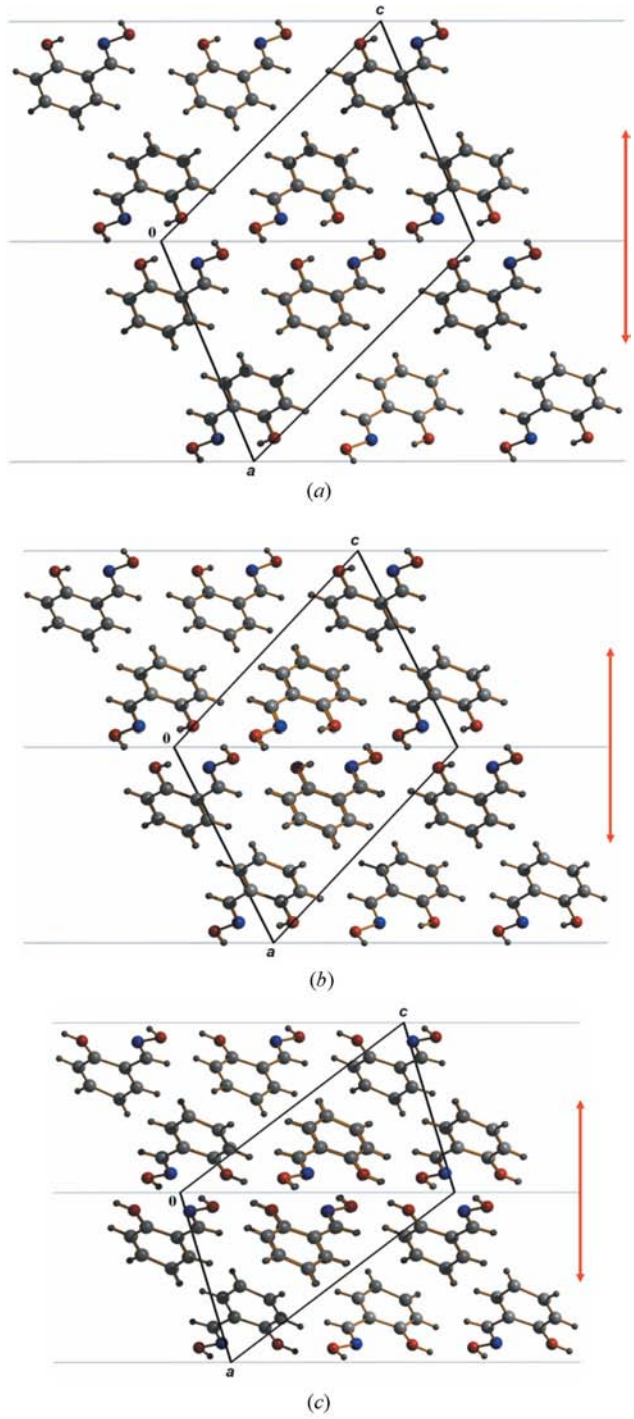

Figure 3
The effect of pressure on the slabs in the salicylaldoxime structure formed from the *C*(7) chains: (*a*) salicylaldoxime-I at ambient pressure; (*b*) salicylaldoxime-I at 5.28 GPa; (*c*) salicylaldoxime-II at 5.93 GPa. The blue lines shown in the diagram are $(10\bar{1})$ planes viewed side-on. The red arrows indicate the extent of one slab in each diagram. The colour scheme is the same as in Fig. 1.

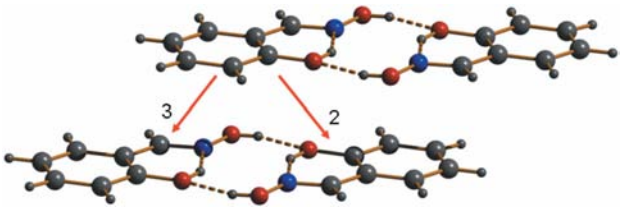

Figure 4
The $\pi\cdots\pi$ stacking interactions between two dimers. Labels 2 and 3 refer to the specific interactions studied using the PIXEL method (*cf.* Fig. 9). The colour scheme is the same as in Fig. 1.

compressed. The distance for interaction 3 in Fig. 4 decreases by 14.8% from 3.40 Å at ambient pressure to 2.90 Å at 5.28 GPa, and the distance for interaction 2 decreases by 8.3% from 3.07 to 2.82 Å at 5.28 GPa. The offset distances for interactions 2 and 3 change from 5.25 to 5.01 Å and from 3.71 to 3.99 Å, respectively, as the molecules slide across each other.

3.3. Salicylaldoxime-II at 5.93 GPa

The observation that the transition from phase I to II proceeds from one single crystal to another suggests that the

Table 2
Non-covalent interaction parameters in salicylaldoxime-I (distances are in Å and angles in °).

Pressure (GPa)	0	0.75	2.37	3.46	4.55	5.28
O5—H5···N2^{i}						
H5···N2	1.91	1.90	1.87	1.83	1.90	1.86
O5···N2	2.621 (2)	2.607 (4)	2.588 (4)	2.580 (4)	2.570 (5)	2.564 (5)
O5—H5···N2	144 (2)	143	145	152	138	144
O1—H1···O5^{ii}						
H1···O5	2.02	1.98	1.92	1.89	1.86	1.83
O1···O5	2.793 (2)	2.753 (6)	2.683 (6)	2.654 (6)	2.630 (7)	2.612 (6)
O1—H1···O5	156 (2)	157	155	154	156	160
C6—H6···O1^{iii}						
H6···O1	2.54	2.44	2.35	2.30	2.27	2.27
C6···O1	3.404 (2)	3.316 (8)	3.169 (8)	3.132 (7)	3.089 (9)	3.077 (9)
C6—H6···O1	154 (1)	150	149	147	147	146
$\pi\cdots\pi^{iv}$ #2						
Plane–plane	3.073 (2)	2.984 (3)	2.872 (3)	2.839 (2)	2.798 (3)	2.819 (3)
Offset	5.25 (1)	5.24 (2)	5.15 (2)	5.10 (2)	5.03 (2)	5.01 (2)
$\pi\cdots\pi^{v}$ #3						
Plane–plane	3.402 (2)	3.289 (3)	3.103 (3)	3.024 (2)	2.957 (3)	2.896 (3)
Offset	3.71 (1)	3.74 (2)	3.84 (2)	3.90 (2)	3.95 (2)	3.99 (2)

Symmetry codes: (i) x, y, z; (ii) $-x, -y, -z$; (iii) $\frac{1}{2}+x, \frac{1}{2}-y, \frac{1}{2}+z$; (iv) $1-x, 1-y, 1-z$; (v) $x, -1+y, z$.

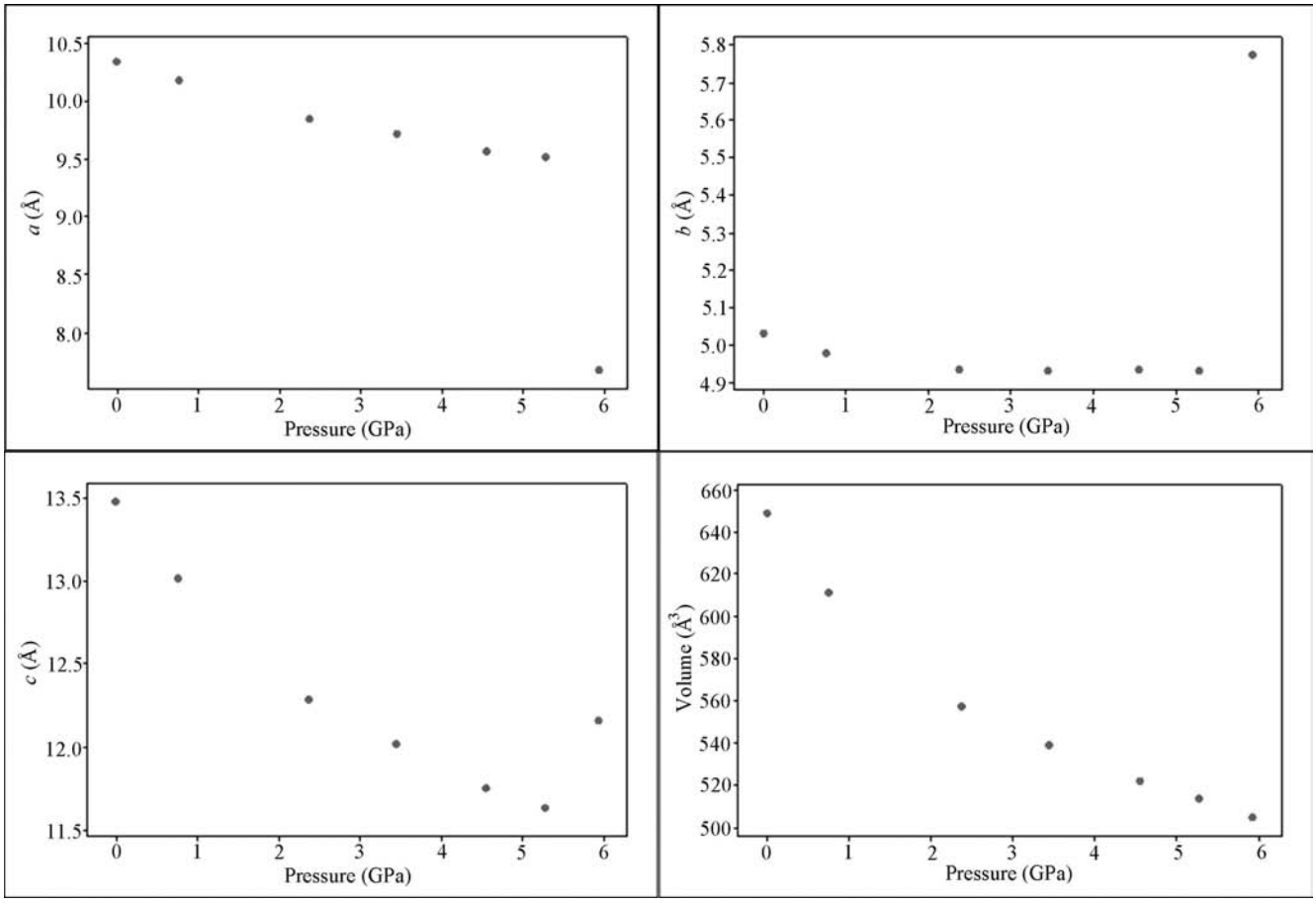

Figure 5
Variation of the lattice parameters (a, b and c, Å) and volume (Å^3) of salicylaldoxime as a function of pressure (GPa).

local topologies of the phase I and II structures are similar to each other. The space-group symmetry is retained, and the cell volume also follows a fairly smooth curve from the ambient-pressure structure through the transition into phase II at 5.93 GPa (Fig. 5).

The $R_4^4(10)$ ring motif found in the phase I structure is no longer present in salicylaldoxime-II. At 5.93 GPa atom H1 forms an O1—H1···N2 hydrogen bond to N2 instead of O5 [O1···N2 = 2.622 (2) Å]. The new OH···N intra-dimer interaction and its inversion-related equivalent form an $R_2^2(6)$ ring motif in the phase II structure (Scheme 2*b* and Fig. 1*c*). This shifting of the molecules in the dimer and formation of an $R_2^2(6)$ instead of an $R_4^4(10)$ ring allows the molecules to approach more closely. The molecules themselves remain planar in the phase II structure; moreover, the two molecules in the dimer are almost exactly coplanar, with a distance of only 0.02 Å between their respective least-squares planes (calculated for each using the C, N and O positions only).

The intramolecular O5—H5···N2 hydrogen bonds found in the phase I structure are also broken and the presence of H1 forming a strong interaction with N2 forces H5 to flip out to the side of the dimer [see Scheme (II)]. This OH group now forms an O5—H5···O1 hydrogen bond to O1 [O5···O1 = 2.582 (14) Å] on a neighbouring molecule in a different dimer, which is related *via* the *n*-glide. These OH···O interactions form *C*(7) chains which run in the direction of the *n*-glide replacing the CH···O *C*(7) chains in the phase I structure. The chains are then linked to each other by the hydrogen bonds across the dimer forming slabs which lie in the $(10\bar{1})$ plane, just as in the ambient pressure structure. There are no hydrogen-bond interactions between the slabs (see Fig. 3*c*).

The $\pi\cdots\pi$ stacking interaction motif found in the salicylaldoxime-I structure is retained in the phase II structure. In the new phase there is still an interaction similar to interaction 3 in Fig. 4, but now the inter-plane separation has increased from 2.90 Å at 5.28 GPa to 3.06 Å at 5.93 GPa and the offset has increased to 4.90 Å. The reference molecule also forms an interaction similar to 2 in Fig. 4, but now the inter-plane separation is 2.91 Å and the offset is 4.87 Å at 5.93 GPa. In the phase II structure the reference molecule phenyl ring is approximately equidistant from the centroids of both phenyl rings in the stacking interaction.

4. Discussion

4.1. Void analysis of the phase I structure

The effect of pressure can be understood in terms of distributions of voids which exist in a structure prior to compression. The voids tend to close up at high pressure, and it is often found that the direction of greatest compressibility in a crystal is directly related to the position and orientation of the largest voids in the structure.

In the salicylaldoxime-I structure it is possible to analyse the distribution and size of structural voids using a Voronoi–Dirichlet analysis as shown by Blatov & Shevchenko (2003) and by Moggach, Allan, Parsons *et al.* (2005). The largest void region (volume 16.77 Å^3) consists of three void conglomerates which lie in between the slabs of the structure. Figs. 7(*a*) and (*b*) show space-filling plots of the salicylaldoxime-I structure,

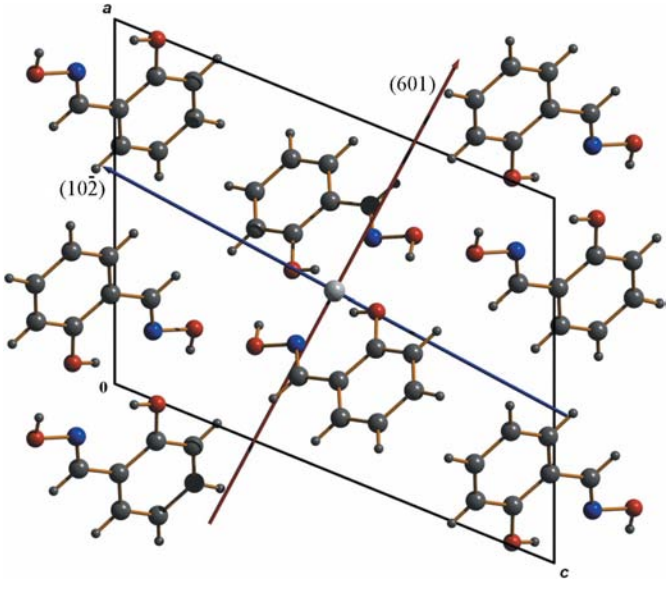

Figure 6
The directions of greatest strain in the salicylaldoxime-I crystal structure between ambient pressure and 5.28 GPa as viewed along *b*. The blue arrow shows the largest eigenvector of the strain tensor, the $(10\bar{2})$ reciprocal axis direction, and the red arrow shows the second largest eigenvector, the (601) reciprocal axis direction. The colour scheme is the same as in Fig. 1.

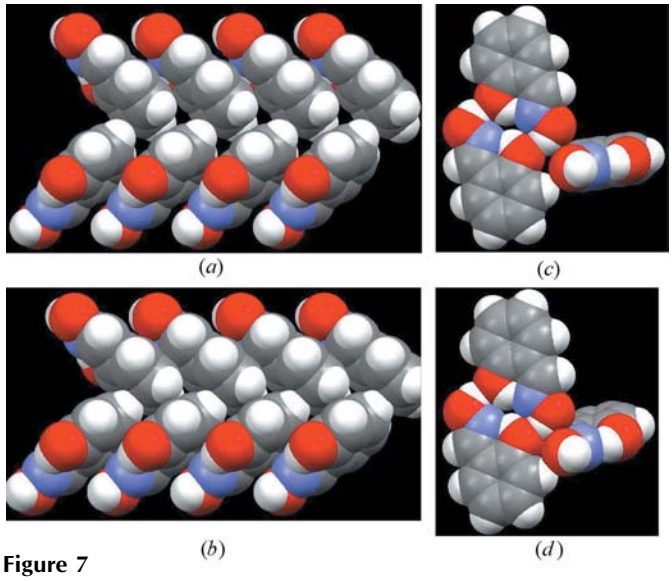

Figure 7
Space-filling plots showing the contraction of voids which occur in salicylaldoxime phase I with the application of pressure. The top and bottom rows correspond to the salicylaldoxime-I structure at ambient pressure and at 5.28 GPa, respectively. (*a*) and (*b*) show the structure with the **a*** direction vertical; there are large voids between the molecules, which almost disappear completely with increasing pressure. (*c*) and (*d*) show the void between molecules related by the *n*-glide; this gap also closes up considerably with the application of pressure.

at ambient pressure and 5.28 GPa, respectively. It is apparent that there is a sizable void between the slabs at ambient pressure which closes up significantly at 5.28 GPa. The direction of movement of the molecules that closes the gap between the slabs is also in the direction of greatest linear strain.

The second largest cluster of voids, which has a volume of 9.50 Å^3, lies between molecules related by the *n*-glide, and this void can be seen in the structures at ambient pressure and 5.28 GPa in Figs. 7(*c*) and (*d*). The gap relates to the relatively long C6—H6···O1 weak hydrogen-bond interaction. The vector between C6 and O1 corresponds approximately to the second direction of greatest strain in the structure (the angle between the vectors is 12°).

The void in the middle of the hydrogen-bonded dimer is formed by relatively strong hydrogen bonds, and it would not be expected to compress as much as voids in the vicinity of more weakly interacting molecules. Nevertheless, the dimer cavity is affected by the application of high pressure. The size of the cavity can be analysed by measuring the mean distance of the donor atoms from the centroid of the dimer. This distance decreases steadily with pressure from 2.0048 (15) to 1.935 (4) Å at 5.28 GPa, as shown in Fig. 8. Smith *et al.* (2002) showed that the cavity size is 1.93 (1) Å in the Cu^{2+} salicylaldoxime complex, whereas in the corresponding Ni^{2+} complex it is 1.864 (1) Å, a change of 0.066 Å. Pressure affects the cavity size by a similar amount. If the size of the cavity can be modified by an amount comparable to the difference in sizes in the different metal complexes, then it is possible that compression may affect the complexation properties of the compound.

Voronoi–Dirichlet analysis shows that the voids present in salicylaldoxime-II are much smaller than those in phase I. There are still small voids between the slabs in the structure, although the majority are distributed between the molecules related by a unit-cell translation in the **b** direction.

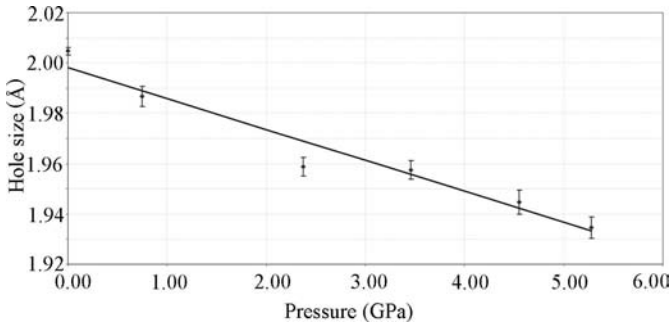

Figure 8
A graph of hole size in salicylaldoxime-I as a function of pressure where the hole size is defined as the mean distance of donor atoms from the centroid of the dimer. The error bars are displayed at the 1σ level.

4.2. Hydrogen bonding and $\pi\cdots\pi$ stacking in salicylaldoxime-I

The three different hydrogen bonds in salicylaldoxime-I do not compress uniformly. The largest compressibility is witnessed for C6—H6···O1, which is the longest hydrogen bond in the structure. Our PIXEL calculations (see below) show that this interaction contributes rather little to the lattice energy at ambient or high pressure, and its distance can be varied without incurring a significant energy penalty. The least compressible hydrogen bond is the intramolecular O5—H5···N2 interaction, which only decreases by a small amount (2.2%) because of the conformational inflexibility of the molecule.

The compression of the intermolecular O1—H1···O5 hydrogen bond is not restricted by the molecular conformation and its compressibility is higher (6.5%) than that of the

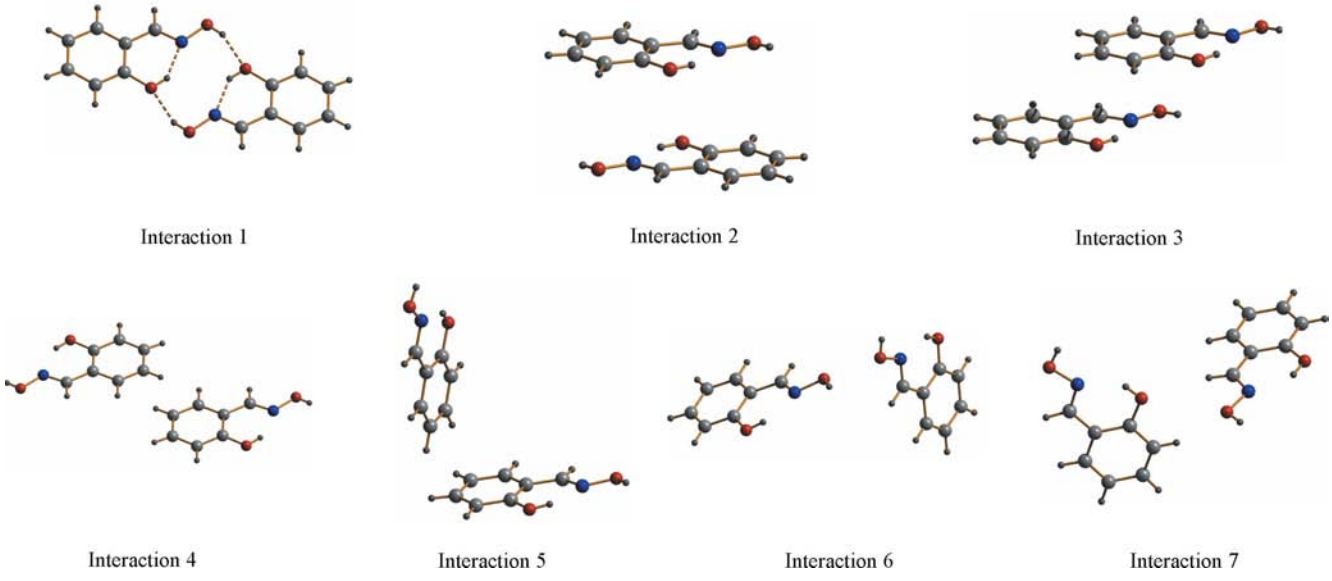

Figure 9
Diagrams of the highest-energy interactions in the salicylaldoxime-I structure from PIXEL analysis.

Table 3
Non-covalent interaction parameters in salicylaldoxime-II at 5.93 GPa (distances are in Å and angles in °).

O1—H1···N2^{i}	
H1···N2	1.85
O1···N2	2.622 (25)
O1—H1···N2	156
O5—H5···O1^{ii}	
H5···O1	1.83
O5···O1	2.582 (14)
O5—H5···O1	151
$\pi\cdots\pi^{iii}$ #2	
Plane–plane	2.925 (10)
Offset	4.86 (4)
$\pi\cdots\pi^{iv}$ #3	
Plane–plane	3.065 (10)
Offset	4.89 (4)

Symmetry codes: (i) $-x, -y, -z$; (ii) $\frac{1}{2}+x, \frac{1}{2}-y, \frac{1}{2}+z$; (iii) $1-x, 1-y, 1-z$; (iv) $x, -1+y, z$.

O5—H5···N2 bond. A search of the CSD revealed the shortest O···O distance in C═NOH···OHC-containing systems to be 2.596 Å [for *rac*-2,3:6,7-dibenzobicyclo(3.3.1)-nona-2,6-diene-4,8-dione dioxime methanol solvate, CSD refcode WUHGEL01; Levkin *et al.*, 2003]. The O···O distance in salicylaldoxime at 5.28 GPa [2.612 (6) Å] is thus near the lower limit observed for such interactions.

The compression of $\pi\cdots\pi$ stacking interactions with hydrostatic pressure has not been extensively studied. Analysis of aromatic stacking interactions in the CSD shows that the minimum stacking distance between phenyl rings is *ca* 2.9 Å. At 5.28 GPa the stacking distances for interactions 2 and 3 (see Fig. 4) are 2.82 and 2.90 Å, respectively. As in the case of the O1—H1···O5 interaction, therefore, the $\pi\cdots\pi$ stacking in salicylaldoxime-I at 5.28 GPa is very close to the lower limit of similar interactions found at ambient pressure. The phase transition to salicylaldoxime-II allows the $\pi\cdots\pi$ stacking distances to increase (inter-planar distances = 2.91 and 3.05 Å), thus reducing the repulsion terms.

Previous compression studies on small organic molecules that exhibit hydrogen bonding, such as glycine (Dawson *et al.*, 2005), L-serine (Moggach, Allan, Morrison *et al.*, 2005) and L-cysteine (Moggach *et al.*, 2006), have shown that the application of hydrostatic pressure (below about 10 GPa) will not decrease the length of a hydrogen bond or other interaction to lower than can be found for similar types of contact in ambient-pressure structures. Once a contact reaches its lower limit a phase transition occurs. The salicylaldoxime-I structure at 5.28 GPa has reached a point where one hydrogen bond and the $\pi\cdots\pi$ stacking interactions have contracted to near their lower distance limits. Further compression of the structure and the reduction of the void found in the middle of the $R_4^4(10)$ ring can only occur through a phase transition, and so above 5.28 GPa salicylaldoxime-II is formed.

The hydrogen-bonding pattern in salicylaldoxime-II is quite different from the ambient phase (Figs. 1 and 2). The intramolecular O5—H5···N2 hydrogen bond is broken in favour of a new intermolecular O5—H5···O1 interaction, while the dimer-forming hydrogen bond (O1—H1···O5) is also broken in order to create a smaller ring without a cavity through a new O1—H1···N2 contact. Overall this yields a more compact structure, although the data in Table 3 and CSD searches show that the new hydrogen bonds are still near the lower limit for their contact types. However, the changes that occur in the distances characterizing the $\pi\cdots\pi$ interactions before and after the phase transition suggest that strain is relieved in this region of the structure.

4.3. PIXEL analysis

In the foregoing discussion we have presented an analysis of the changes that occur in the crystal structure of salicylaldoxime based on intermolecular distances. The PIXEL procedure, which has been developed recently by Gavezzotti, enables further insight to be gained by calculation of intermolecular interaction energies. The method also enables these energies to be broken down into electrostatic, polarization, dispersion and repulsion contributions. In a PIXEL calculation the electron density in an isolated molecule is first calculated using a quantum mechanical package such as *GAUSSIAN*. This electron-density model is then placed in a crystal structure and divided into pixels of electron density. Each energy term is obtained by summing over energies calculated between pairs of pixels in neighbouring molecules. Details on the PIXEL method have been given by Dunitz & Gavezzotti (2005) and Gavezzotti (2005).

The lattice energies and a breakdown of the energies into component coulombic, polarization, dispersion and repulsion terms for each pressure were calculated and are shown in Table 4. The overall lattice energy becomes more positive as pressure is increased; this trend is due to the steady increase in the repulsion term as the molecules are pushed closer together. The phase transition between 5.28 and 5.93 GPa results in a considerable decrease in the overall lattice energy. By extrapolation of the trend established up to 5.28 GPa we estimate that salicylaldoxime-II is more stable than salicylaldoxime-I by approximately 25 kJ mol^{-1} at 5.93 GPa. The energy difference is due to significant decreases in the coulombic and polarization terms, which outweigh the increase in repulsion.

Seven pairs of molecules have interaction energies greater than 2.5 kJ mol^{-1}. These pairs, shown in Fig. 9, have been labelled 1–7 in descending order of their total energies at ambient pressure. The total energies of the pairs at each pressure up to 5.28 GPa are also given in Table 5. The strongest interaction (1) corresponds to the O1—H1···O5 hydrogen-bonded dimer across the inversion centre; this interaction is dominated by the coulombic term, as expected for a hydrogen bond. It continues to be the most important interaction with increasing pressure. The next two strongest interactions (2 and 3) are the $\pi\cdots\pi$ stacking interactions between the reference molecule and two salicylaldoxime units forming a hydrogen-bonded dimer. Each interaction has an energy in the region of 8–9 kJ mol^{-1}, with a large dispersion

Table 4
Components of lattice energy and total energy at each pressure (GPa) for salicylaldoxime (energies in kJ mol^{-1}).

Pressure	Coulombic	Polarization	Dispersion	Repulsion	Total energy
0.00	−56.4	−22.1	−87.5	78.2	−87.9
0.75	−65.8	−27.5	−101.5	109.4	−85.4
2.37	−95.9	−44.0	−128.4	190.3	−78.0
3.46	−107.2	−48.9	−137.0	226.5	−66.5
4.55	−121.7	−57.7	−147.9	275.9	−51.4
5.28	−128.3	−65.7	−154.0	304.2	−43.8
5.93	−221.1	−117.2	−163.9	443.0	−59.2

Table 5
Total energies of the seven strongest interactions with increasing pressure (GPa) in salicylaldoxime-I (energies in kJ mol^{-1}).

Pressure	0.00	0.75	2.37	3.46	4.55	5.28
Interaction 1	−25.0	−24.2	−23.4	−20.6	−17.5	−17.6
Interaction 2	−8.7	−8.8	−7.6	−7.3	−5.9	−5.8
Interaction 3	−8.1	−8.3	−7.5	−5.6	−4.3	−2.8
Interaction 4	−6.2	−6.4	−6.6	−5.8	−6.0	−5.6
Interaction 5	−4.8	−4.6	−3.1	−2.5	−1.6	−1.2
Interaction 6	−4.0	−3.9	−3.9	−3.6	−2.6	−1.4
Interaction 7	−2.7	−2.5	−1.5	−1.0	0.1	0.1

component. Interactions 4, 5 and 6 would all be overlooked in a conventional analysis focusing on hydrogen bonding, but each has an overall attractive interaction, amounting to between 4 and 7 kJ mol^{-1}. These interactions are an H···H contact, an offset CH···π interaction and an O···O contact, respectively. Interaction 7 corresponds to the C6—H6···O1 hydrogen bond discussed above. It seems that this 'weak hydrogen-bonding' interaction contributes very little to the overall lattice energy, and has more contribution from the dispersion component than the coulombic component.

The data from structures at increasing pressures show that each interaction becomes weaker as a result of the increasing repulsion terms. The responses of the interactions to hydrostatic pressure are by no means uniform, and Fig. 10 shows a graph of the total interaction energies for each of the seven principal interactions against the distance between the molecular centroids of the two molecules involved in the interaction. The data shown in Fig. 10 were also calculated using the Gavezzotti force-field [available in the program *RPLUTO* (Motherwell, 2002)] yielding qualitatively similar results.

Interactions 2, 4, 5, 6 and 7 are relatively unaffected by the compression. The interactions between these pairs of molecules would therefore seem to be very soft and not influential in the forcing of the phase transition. In contrast, the curves for interactions 1 and 3 are much steeper (note the distinct difference between the two stacking interactions 2 and 3). These results are consistent with the suggestion made above that the phase transition occurs in order to avoid further shortening of the OH···O hydrogen bond and π···π stacking distances. These results also suggest that the π···π interactions become strongly repulsive upon shortening and would appear to be very important in both the phase I structure and the phase transition to salicylaldoxime-II.

The energies of interactions in the phase II structure were also analysed using the PIXEL method. The most energetically stabilizing interaction, as expected, is the $R_2^2(6)$ hydrogen-bonded ring. The pair of molecules involved has a total interaction energy of −16 kJ mol^{-1}, which is comparable to that of the phase I dimer interaction energy at 5.28 GPa.

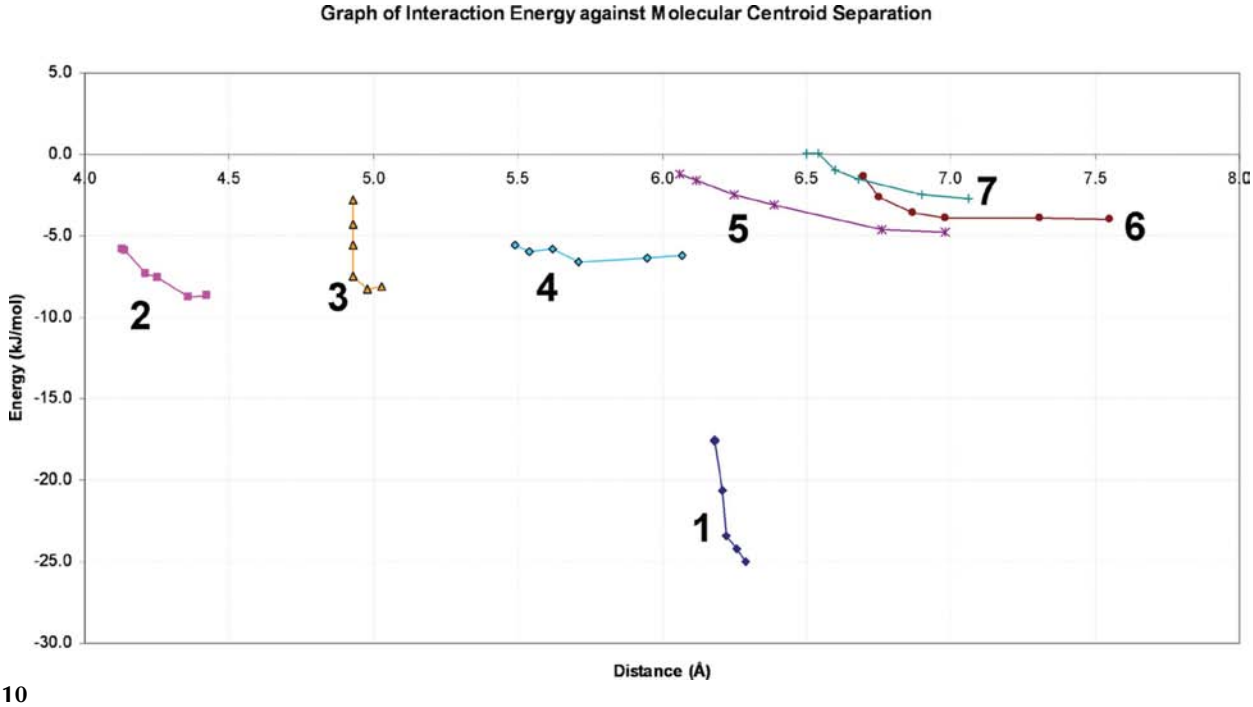

Figure 10
Graph of the total interaction energy (in kJ mol^{-1}) against the distance between the molecular centroids of the molecules involved in the interaction (in Å).

Other significant interactions include $\pi\cdots\pi$ interactions similar to those found in the phase I structure, which have total interaction energies of −5.5 and −4.3 kJ mol^{-1}.

The hydrogen bond O5—H5$\cdots$O1, which was formed by conversion of an intramolecular hydrogen bond into an intermolecular hydrogen bond, is found to have a large attractive coulombic term (−35.6 kJ mol^{-1}), but is actually not an attractive interaction overall (E_{tot} = +1 kJ mol^{-1}) owing to the high value for the repulsion term (57.6 kJ mol^{-1}). It seems that the intra- to intermolecular hydrogen-bond conversion has allowed a pair of molecules to approach one another in order to pack more efficiently.

5. Conclusions

We have described here the effects of the application of hydrostatic pressure on the structure of salicylaldoxime. The principal effects of pressure, up to 5.28 GPa, on the phase I structure are to close up the voids present in the ambient pressure structure by shortening the intermolecular interactions and moving the non-hydrogen-bonding slabs closer together. The only void in the ambient-pressure structure that is still visible in a space-filling plot at 5.28 GPa is in the middle of the $R_4^4(10)$ hydrogen-bonding ring which binds the salicylaldoxime molecules into dimers.

The pseudo-macrocyclic cavity in the salicylaldoxime dimer has been shown to decrease in size steadily with the application of hydrostatic pressure. This contraction of the cavity size is comparable to the difference in the hole sizes in the copper and nickel salicylaldoxime complex structures. The results suggest that it may be possible to tune the metal-complex formation selectivity of the salicylaldoximes using high pressure.

The intermolecular hydrogen bonds and $\pi\cdots\pi$ interactions in the structure are compressed at 5.28 GPa to the lower limits of similar contacts at ambient pressure found in a search of the CSD. PIXEL calculations show a concomitant sharp increase in the repulsion energy of these interactions. Phase I is stable up to 5.28 GPa, but beyond this pressure the structure transforms to a new polymorph – salicylaldoxime-II. The phase II structure breaks the $R_4^4(10)$ hydrogen-bonded ring in favour of an $R_2^2(6)$ ring, which only has two hydrogen bonds, in order to improve the packing of the molecules. A CH$\cdots$O interaction is also replaced by an OH$\cdots$O hydrogen bond; overall this interaction is actually very slightly repulsive, but the intra- to intermolecular hydrogen-bond conversion enables a pair of molecules to approach one another in order to promote more efficient packing.

We are very grateful to Professor Angelo Gavezzotti (University of Milan) for his help and advice with our PIXEL calculations. We also thank the EPSRC and The Cambridge Crystallographic Data Centre for funding, and the CCLRC for provision of synchrotron beam-time.

References

Allen, F. H. (2002). *Acta Cryst.* B**58**, 380–388.
Allen, F. H. & Motherwell, W. D. S. (2002). *Acta Cryst.* B**58**, 407–422.
Altomare, A., Cascarano, G., Giacovazzo, C., Guagliardi, A., Burla, M. C., Polidori, G. & Camalli, M. (1994). *J. Appl. Cryst.* **27**, 435.
Angel, R. (2000). *Rev. Mineral. Geochem.* **41**, 35–59.
Angel, R. (2002). *EOSFIT*, Version 5.2. Virginia Tech., Blackburg, VA, USA.
Angel, R. (2004). *High Pressure Crystallography*, NATO Science Series II, edited by A. Katrusiak & P. McMillan, pp. 21–36. Dordrecht: Kluwer Academic Publishers.
Bernstein, J., Davis, R. E., Shimoni, L. & Chang, N-L. (1995). *Angew. Chem. Int. Ed. Engl.* **34**, 1555–1573.
Betteridge, P. W., Carruthers, J. R., Cooper, R. I., Prout, K. & Watkin, D. J. (2003). *J. Appl. Cryst.* **36**, 1487.
Birch, F. (1947). *Phys. Rev.* **71**, 809–824.
Blatov, V. A. (2005). *TOPOS Manual.* Samara State University, Russia.
Blatov, V. A. & Shevchenko, A. P. (2003). *Acta Cryst.* A**59**, 34–44.
Blatov, V. A., Shevchenko, A. P. & Serezhkin, V. N. (1995). *Acta Cryst.* A**51**, 909–916.
Blatov, V. A., Shevchenko, A. P. & Serezhkin, V. N. (2000). *J. Appl. Cryst.* **33**, 1193.
Boldyreva, E. V. (2003). *J. Mol. Struct.* **647**, 159–179.
Boldyreva, E. V. (2004*a*). *J. Mol. Struct.* **700**, 151–155.
Boldyreva, E. V. (2004*b*). *Mathematics, Physics and Chemistry*, NATO Science Series, II, edited by A. Katrusiak & P. F. McMillan, Vol. 140, pp. 495–512. Dordrecht: Kluwer Academic Publishers.
Brandenburg K. & Putz H. (2005). *DIAMOND*. Crystal Impact, Bonn, Germany.
Bruker–Nonius (2000). *APEX*-II. Bruker–Nonius, Madison, Wisconsin, USA.
Bruker–Nonius (2003). *SAINT*, Version 7. Bruker AXS Inc., Madison, Wisconsin, USA.
Bruno, I. J., Cole, J. C., Edgington, P. R., Kessler, M., Macrae, C. F., McCabe, P., Pearson, J. & Taylor, R. (2002). *Acta Cryst.* B**58**, 389–397.
Dawson, A., Allan, D. R., Belmonte, S. A., Clark, S. J., David, W. I. F., McGregor, P. A., Parsons, S., Pulham, C. R. & Sawyer, L. (2005). *Cryst. Growth Des.* **5**, 1415–1427.
Dawson, A., Allan, D. R., Parsons, S. & Ruf, M. (2004). *J. Appl. Cryst.* **37**, 410–416.
Dunitz, J. D. & Gavezzotti, A. (2005). *Angew. Chem. Int. Ed.* **44**, 1766–1787.
Farrugia, L. J. (1999). *J. Appl. Cryst.* **32**, 837–838.
Frisch, M. J. *et al.* (1998). *GAUSSIAN*98, Revision A.7. Gaussian Inc., Pittsburgh, PA, USA.
Gavezzotti, A. (2005). *Z. Kristallogr.* **220**, 499–510.
Gokel, G. W. (1991). *Crown Ethers and Cryptands.* Cambridge, UK: Royal Society of Chemistry.
Hazen, R. M. & Finger, L.W. (1982). *Comparative Crystal Chemistry*, p. 81. Chichester: John Wiley and Sons.
Hemley, R. J. & Dera, P. (2000). *Rev. Mineral. Geochem.* **41**, 335–419.
Katrusiak, A. (2004). *Mathematics, Physics and Chemistry*, NATO Science Series II, edited by A. Katrusiak & P. F. McMillan, Vol. 140, pp. 513–520. Dordrecht: Kluwer Academic Publishers.
Kordosky, G. A. (2002). *Proceedings of the International Solvent Extraction Conference*, Cape Town, South Africa, 17–21 March 2002, pp. 853–862. South African Institute of Mining and Metallurgy, Johannesburg, South Africa.
Levkin, P. A., Lyssenko, K. A., Schurig, V. & Kostyanovsky, R. G. (2003). *Mendeleev Commun.* pp. 106–108.
Merrill, L. & Bassett, W. A. (1974). *Rev. Sci. Instrum.* **45**, 290–294.
Merritt, L. L. & Schroeder, E. (1956). *Acta Cryst.* **9**, 194.
Moggach, S. A., Allan, D. R., Clark, S. J., Gutmann, M. J., Parsons, S., Pulham C. R. & Sawyer, L. (2006). *Acta Cryst.* B**62**, 296–309.

Moggach, S. A., Allan, D. R., Morrison, C. A., Parsons, S. & Sawyer, L. (2005). *Acta Cryst.* B**61**, 58–68.
Moggach, S. A., Allan, D. R., Parsons, S., Sawyer, L. & Warren, J. E. (2005). *J. Synchrotron Rad.* **12**, 598–607.
Motherwell, S. (2002). *RPLUTO*. Cambridge Crystallographic Data Centre, UK.
Parsons, S. (2003). *STRAIN*. The University of Edinburgh, Scotland.
Parsons, S. (2004). *SHADE*. The University of Edinburgh, Scotland.
Pfluger, C. E. & Harlow, R. L. (1973). *Acta Cryst.* B**29**, 2608–2609.
Piermarini, G. J., Block, S., Barnett, J. D. & Forman, R. A. (1975). *J. Appl. Phys.* **46**, 2774–2780.
Press, W. H., Teukolsky, S. A, Vetterling, W. T. & Flannery, B. P. (1992). *Numerical Recipes in Fortran*, 2nd ed. Cambridge University Press.
Prince, E. (1982). *Mathematical Techniques in Crystallography and Materials Science*. Springer-Verlag, New York.
Sheldrick, G. M. (2004). *SADABS*. Bruker AXS Inc., Madison, Wisconsin, USA.
Slebodnick, C., Zhao, J., Angel, R., Hanson, B. E., Song, Y., Liu, Z. & Hemley, R. J. (2004). *Inorg. Chem.* **43**, 5245–5252.
Smith, A. G., Tasker, P. A. & White, D. J. (2002). *Coord. Chem. Rev.* **241**, 61–85.
Spek, A. L. (2004). *PLATON*. Utrecht University, The Netherlands.
Szymanowski, J. (1993). *Hydroxyoximes and Copper Hydrometallurgy*. Boca Raton: CRC Press.
Tasker, P. A., Plieger, P. G. & West, L. C. (2004). *Comprehensive Coordination Chemistry II*, Vol. 9, pp. 759–808. Amsterdam: Elsevier.
Watkin D. J. (1994). *Acta Cryst.* A**50**, 411–437.
Watkin, D. J., Pearce, L. & Prout, C. K. (1993). *CAMERON*. Chemical Crystallography Laboratory, University of Oxford, England.
Wood, P. A., Forgan, R. S., Parsons, S., Pidcock, E. & Taskev, P. A. (2006). *Acta Cryst.* E**62**, o3944–o3946.